

11-1-2016

Dust Devil Populations and Statistics

Ralph D. Lorenz
Johns Hopkins University

Brian K. Jackson
Boise State University

Dust Devil Populations and Statistics

Ralph D. Lorenz

Applied Physics Laboratory
Johns Hopkins University
Laurel, MD

Brian K. Jackson

Department of Physics
Boise State University
Boise, ID

Abstract

The highly-skewed diameter and pressure drop distributions of dust devils on Earth and Mars are noted, and challenges of presenting and comparing different types of observations are discussed. The widely-held view that Martian dust devils are larger than Earth's is critically-assessed: the question is confounded somewhat by different observation techniques, but some indication of a ~3x larger population on Mars is determined. The largest and most intense (in a relative pressure sense) devils recorded are on Mars, although the largest reported number density is on Earth. The difficulties of concepts used in the literature of 'average' diameter, pressure cross section, and area fraction are noted in the context of estimating population-integral effects such as dust lifting.

1. Introduction

Dust devils are a prominent feature of meteorology on Mars and in desert areas on the Earth. They are responsible for dust-lifting on both Earth and Mars, for surface albedo changes on Mars which may give rise to interannual climate variability, for the clearing of dust from the solar panels of landers and rovers, and for occasional death, injury and damage on Earth. The question of 'how many dust devils are there?' is therefore an important one but requires some rigor and subtlety in answering. It is, for example, commonly considered that dust devils are larger on Mars than on Earth – but how much of that perceived distinction is due to the very different instruments and techniques used to evaluate the populations? Some rational approaches to the presentation of dust devil population data are suggested to help manage the difficulties of evaluating and comparing highly-skewed populations.

2. Definition and Representation

Before discussing observations of an inferences about the population of dust devils in different environments, it is important first to establish a working definition of the objects under study (and later we will introduce quantitative criteria). We also lay some groundwork in this section on the styles of data presentation to be used later.

2.1 Dust Devil Definition

A Venn Diagram (figure 1) is helpful to describe various phenomena discussed in the context of dust devils. While there are many visible clouds of dust in desert areas, not all are dust devils. Similarly, there exist many dry columnar vortices in the planetary boundary layer, but not all carry dust. The two essential characters of dust devils, namely a columnar vortex and lofted dust, provide the definition. In this respect our definition is slightly wider than Oke et al. (2007) who suggest a specific criterion for circumferential windspeed, diameter, and duration: *"A vortex rotating in either direction faster than its motion downwind. It must have a coherent columnar or cone shape extending in a vertical direction above the surface. It must carry dust to a height of at least 1m and last for at least 10 s. It is distinct from a dust blow in that it maintains a fast rotating coherent structure with vertical extension and distinct from a small dust whirl in its size and duration."* It is useful to keep this alternative definition in mind when considering the rest of this paper in so far as it represents an example of a heuristic set of criteria for counting

features observed in the field. We will discuss later other quantitative criteria in the context of automatic detection of features in meteorological time series, images, or simulated fields of meteorology data. We may note also in figure 1 that features of dust devil populations can be inferred from studies of dust devil tracks (discussed in a later section, and in the companion chapter by Reiss et al.), but such tracks are formed only by a subset of dust devils.

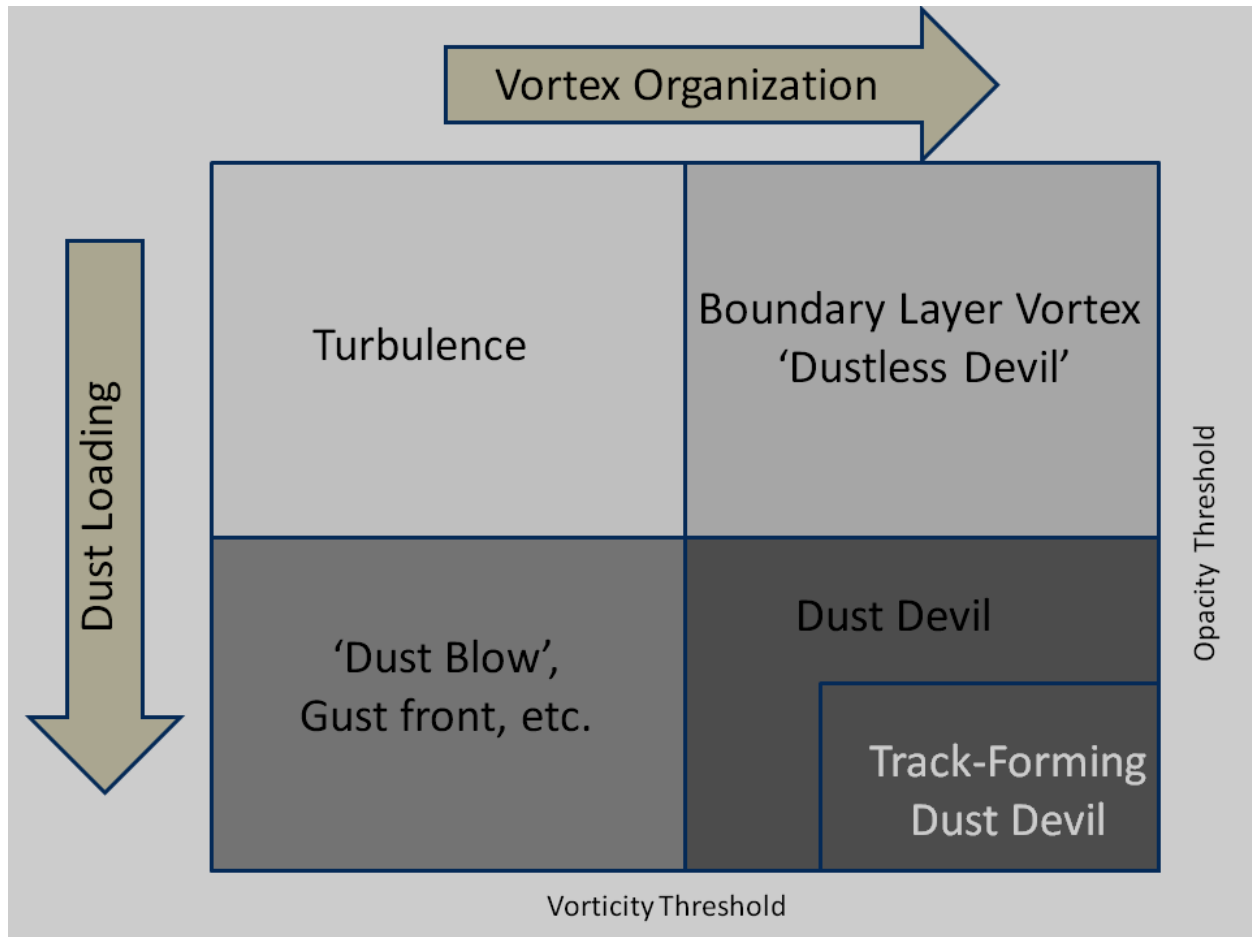


Figure 1. Schematic categorization of events. 'Intensity' is in essence a combination of the organization and strength of a wind or pressure perturbation, and is a maximum in the lower right part of the plot. Small fluctuations always exist in the turbulent windfield, which can sometimes raise dust in a less organized way ('dust blows') in the lower left. Well-organized vortices often exist without lofted dust, where the dust-lifting threshold is high, for example, but can be detected with meteorological instrumentation, yielding events in the upper right. When dust is lifted by a vortex, we see the classic 'dust devil', a subset of which can form trails on the ground.

2.2 Presentation of Population Data

Having established that some criterion is needed to 'count' entities such as dust devils, we now make some general remarks that may be made on the presentation of dust devil counts, echoing discussion in Lorenz (2011, 2012).

Although historically visual counts in the field have of necessity been classified in three or four size bins, in general, binning is to be avoided ("Binning is sinning") since information is lost. If it must be done, then ideally an information-theoretic criterion might be used in bin-size selection (e.g. Jackson and Lorenz, 2015), or at least binning be done in some manner well-suited to strongly skewed data e.g. logarithmically (bins of size ratio equal to the square root of two, as used often in the impact cratering community, is one approach). Cumulative plots have some virtues, not least in making noisy data look somewhat smoother – e.g. figure 2. Because cumulative plots can

integrate out some details (since they have a wide dynamic range), a cumulative plot normalized to some function such as a power law can be useful (e.g. in the impact cratering literature, crater counts normalized to a -2 power law is referred to as an ‘R-plot’ (Melosh, 1990) and indicates the relative area covered by craters of a given diameter).

The problem of how to estimate densities and bin data has a long history in the data science and machine-learning literature and comes down to striking the right balance between using few enough bins to smooth out statistical fluctuations without removing important trends in the data. Many solutions have been developed to address this problem, ranging from simple rules-of-thumb to more sophisticated procedures based on Bayesian analysis of the data. For instance, the recently developed Bayesian Blocks scheme (Scargle et al. 2013) aims for this balance by increasing the number of bins to minimize variations within a bin, while incorporating a penalty each time a new bin is added. Many binning routines are readily available via open-source scientific computing modules such as scikit-learn (<http://scikit-learn.org/stable/modules/density.html>) and astroml (http://www.astroml.org/user_guide/density_estimation.html).

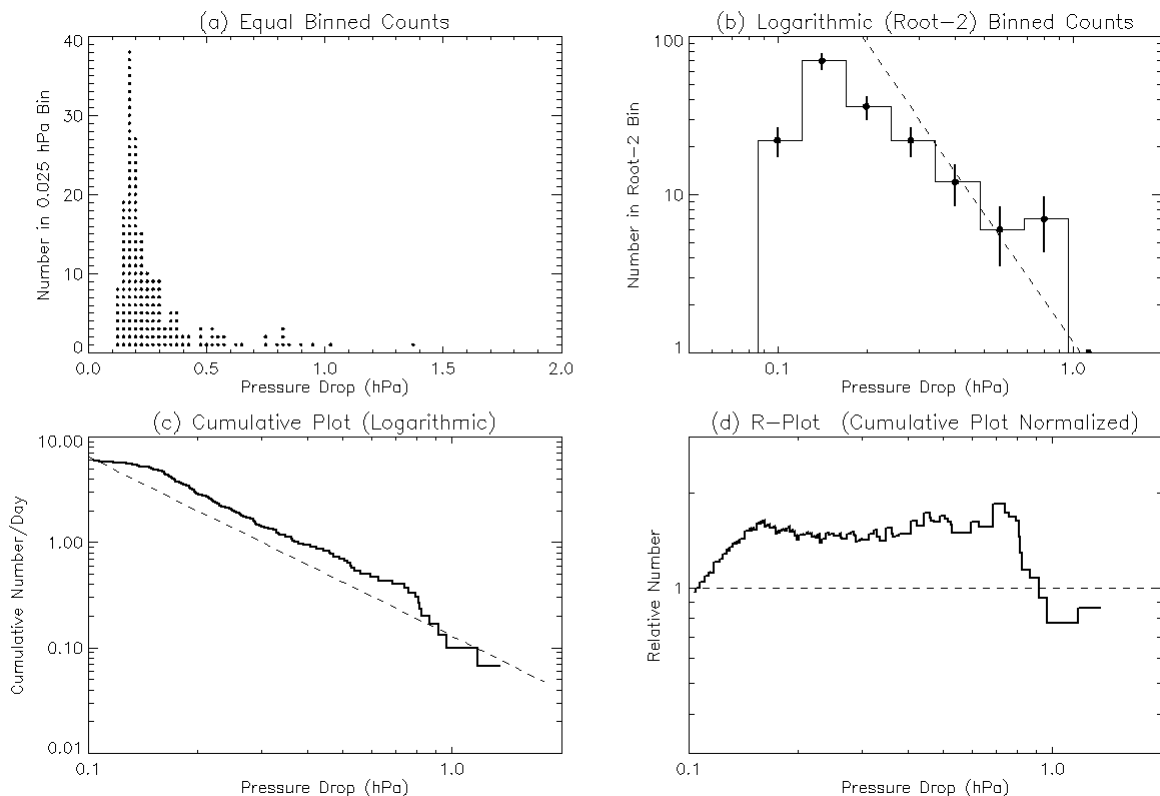


Figure 2. Different ways of presenting the same data, the ‘P28’ dataset of dust devil pressure drops measured in a 30-day period at El Dorado by Lorenz and Lanagan (2014). Many visual surveys have presented data as simple linear equal-bin histograms or counts, similar to (a). The widely different number of counts at small and large sizes makes it difficult to assimilate the population function, and the statistics at the large end are poor. That issue can be addressed by using logarithmic binning, with bins having an equal ratio, rather than difference, in threshold. A $\sqrt{2}$ ratio is often a good compromise between retaining enough datapoints to define the function shape, while keeping enough counts in each bin to avoid large counting errors except in the last bin. However, by using a cumulative count, binning can be avoided altogether, as in (c). The staircase appearance is due to poor statistics at the large end, but is faithful to the data. For comparing different datasets, it may be useful to normalize the cumulative function by an analytic expression to obtain a relative rate, in this case an entirely empirical function $R(>P) = (P/0.3)^{-1.7}$, shown by the dashed line in (c) and (d) is used. This normalization (in the impact-cratering literature, referred to as an ‘R-plot’ where the normalization exponent is 2.0) reduces the dynamic range required in the y-axis, and therefore exposes differences more clearly.

Whether binned or not, and shown in a differential or cumulative manner, a variety of analytic functions may be used to describe or parameterize the distribution. Kurgansky (2006) suggested an exponential model fitted the crudely-binned statistics of Sinclair's Tucson survey, whereas Lorenz (2009) showed that the Mars diameters measured by Greeley et al. (2006) on the Spirit rover were better-fit by a (truncated) power law. Further discussion by Pathare (2010) advocated an exponential model for some terrestrial field data, but this was challenged by Lorenz (2011), who cautioned that the coarse binning and poor statistics challenged the significance of selection of one analytical model against another. The one exception to date appears to be the data from Ryan and Carroll (1970), where 5 size bins were populated. Those data, with bin thresholds of 1.5, 3, 6, 12 and 25m, are 370, 165, 31, 17, 5 devils are quite accurately fit with a power law of -2.6 (i.e. a cumulative power law of -1.6). The question of best function for the Gusev data was revisited by Kurgansky (2012).

Pending the availability of better (unbinned) datasets for Earth, we suggest that the choice of diameter function is something of an aesthetic choice, with log-normal, Weibull, exponential or (truncated) power law functions all likely to give adequate fit to binned data. The power law enjoys some analytic convenience, however.

3. Population Assessment of Dust Devils

3.1 Optical Detections

The survey technique with the longest pedigree is naturally that of observing in the field. As noted by Balme and Greeley (2006), the observed formation rate of dust devils varies with the area surveyed – and the range of reported occurrence rates (from $\sim 0.1 \text{ km}^{-2} \text{ day}^{-1}$ to some $\sim 800 \text{ km}^{-2} \text{ day}^{-1}$) is initially baffling. However, Lorenz (2009) showed that this variation is systematic, with detected rates N (devils $\text{km}^{-2} \text{ day}^{-1}$) being inversely proportional to survey area A (km^2), with $N \sim 50/A$, and suggested that this could be explained by a power law diameter distribution and a detection threshold that varied with distance (and thus survey area – see figure 3). The detection efficiency of small and/or optically-thin devils is essential to take into account, for example in comparing populations observed at different sites, and to understand the shape of the actual dust devil population function (e.g. Lorenz, 2011; Kurgansky, 2012). It may be that for a given survey circumstance, e.g. camera location, there are temporal variations in detection efficiency owing to the different viewing/scattering geometry as a function of time of day, etc.

It is instructive to consider a recent observation in the context of this plot. A first detection of terrestrial dust devils in satellite imaging was described by Reiss et al. (2016) finding as many as 30-40 devils per 1000 km^2 in Landsat and ASTER data, corresponding to diameters of 20-155m. Following the empirical longevity relationship of Lorenz (2013), dust devils in this size last 300-1200s, or about one-sixtieth to one-twentieth of a 'day' of dust devil activity (~ 6 hours). Thus the observed occurrence rate is $0.6\text{-}2.4 \text{ km}^{-2} \text{ day}^{-1}$, corresponding to a survey area equal to the image size of $\sim 1500 \text{ km}^2$. It is seen (figure 2) that this datapoint plots

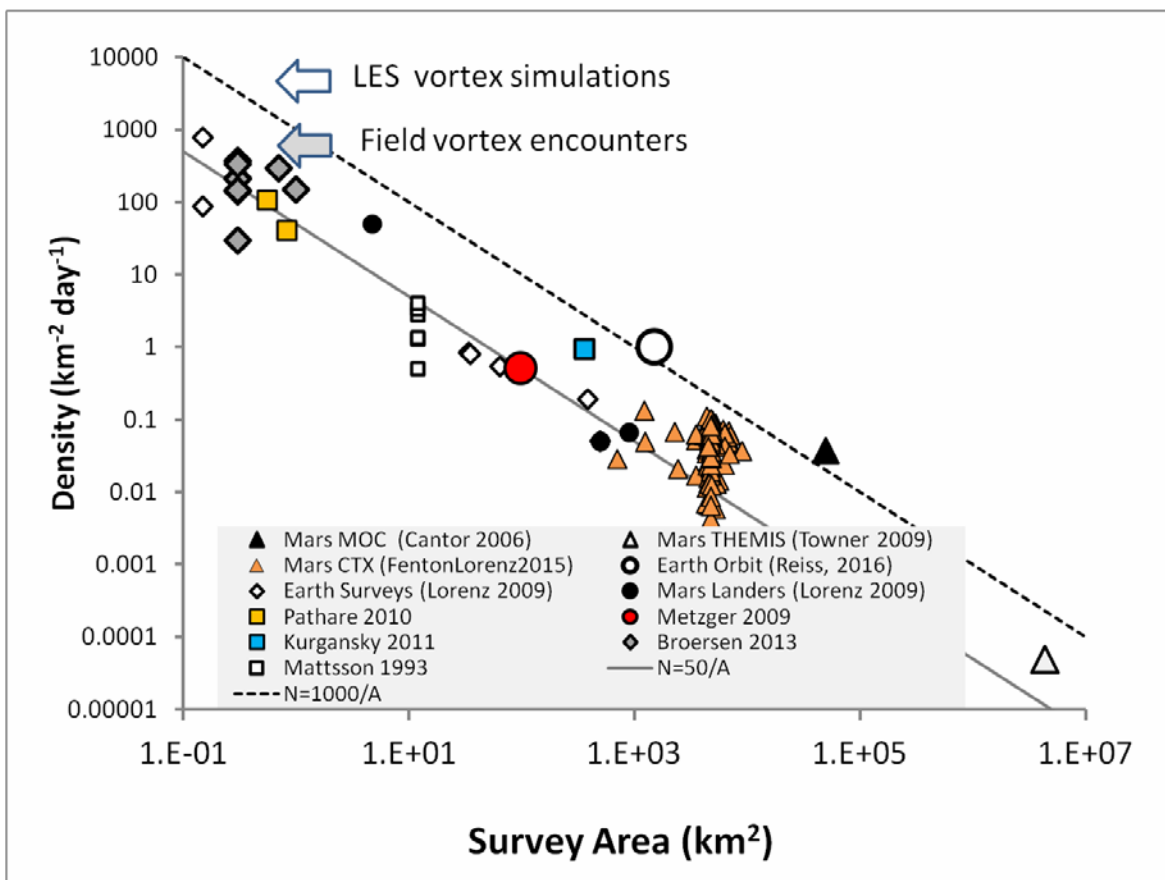


Figure 3. A compilation of observed dust devil frequencies from visual surveys on Earth and Mars, extended from Lorenz (2009,2013). There is a systematic variation of observed counts with area surveyed, presumably because large area surveys (especially those from orbit) only detect the larger, rarer dust devils. Also indicated with a large grey arrow is the vortex generation rate of $300 \text{ km}^{-2} \text{ day}^{-1}$ required, with assumptions on longevity and advection speed, to reproduce in a Monte Carlo model (Lorenz, 2014) the observed vortex pressure dips above 20 Pa seen in terrestrial field data. The vortex formation rate measured in two different terrestrial LES simulations, of $1500\text{-}4500 \text{ km}^{-2} \text{ day}^{-1}$ of 10 Pa and 4 Pa respectively are also shown with a large arrow. Most of these rather weak vortices will be dustless, however. The Mars and Earth rates appear, with survey area taken into account, to be broadly similar: most data fall on a line of $N=50/A$, with the more active sites (and especially, more sensitive observations from orbit) falling on a line of $N=1000/A$.

Figure 3 represents an update of the presentation first adopted in Lorenz (2009) and Lorenz (2013). In addition to the only terrestrial spaceborne imaging (Reiss, 2016) described above, new datapoints shown here are a collection of individual Mars orbital image counts from Fenton and Lorenz (2016) described later in this paper, and field surveys in Jordan (Broersen, 2013), Eldorado playa in Nevada (a ~ 20 day, 300 km^2 survey by Metzger, 2009) and a report from Tunisia by Mattsson et al. (1993).

In this paradigm, generally the smallest areas will have the highest detection rates as 100% of even the smallest devils will be detected and the inventory can be considered ‘complete’¹. The highest observed rates reported in the field are those by Carroll and Ryan (1970) who encountered some 1151 devils in 10 days in a 0.15 km^2 area, or 767

¹ ‘Complete’ in the sense of detecting all devils present in the survey area. Surveys in small areas may statistically encounter less than one devil for large sizes and so are not ‘complete’ in the sense of fully characterizing the population unless they are conducted for a long enough period – see Lorenz (2011). Note that a true power law has no limit, and so there are an infinite number of infinitely small dust devils, which is clearly not the case. In practice there is a lower limit, suggested to be the Obukhov scale or $\sim 1 \text{ m}$ for typical conditions on Earth.

devils $\text{km}^{-2} \text{ day}^{-1}$. This count is especially high for a couple of reasons. First, the site was completely clear of vegetation and they ‘groomed’ the desert surface daily (breaking up the surface with a rake), to maximize the availability of dust. This likely reduced the threshold windspeed or pressure drop required for dust lifting (see later). Second, counts in very small study areas are inflated because dust devils that form elsewhere but are advected into the site are counted - for the 0.15km^2 area and the typical sizes (and thus longevities) and windspeeds encountered, the rate at which vortices form in the study area is probably lower by a factor of 2-3 (see Lorenz, 2013, figure 6). Hence we consider their corrected result as a formation rate of ~ 300 devils $\text{km}^{-2} \text{ day}^{-1}$, noting that the vortex intensity threshold for dust-lifting may have been especially low due to the grooming of the surface.

The highest count in more typical field conditions (indeed, at Eldorado playa in Nevada, where the pressure drop data in the next section was obtained) is that by Pathare et al. (2010), of 528 devils in 0.55km^2 in 9 days. However, this period included some less favorable days, with daily counts varying between 18 and 83. Adopting the highest number yields $N=151$ devils observed per km^2 per day, although again this should be reduced by a factor relating to the advection speed. Thus 100 devils $\text{km}^{-2} \text{ day}^{-1}$ is probably about right for the formation rate, and certainly >75 devils $\text{km}^{-2} \text{ day}^{-1}$. Other surveys (see Lorenz, 2011; 2014) have lower counts. Snow and McLelland (1990) report mean counts of ~ 0.5 devils $\text{km}^{-2} \text{ day}^{-1}$ at White Sands missile range, but close inspection of their figure 3 shows that these were very unevenly distributed in the survey area, and one $0.5 \times 0.5\text{km}$ survey plot saw 151 devils in 41 days, or 14 devils $\text{km}^{-2} \text{ day}^{-1}$. This plot was some kilometers from the observer location, suggesting that this number is rather incomplete, and they note that ‘it is likely that less than 10% of whirlwinds in the small category ($<3.3\text{m}$ diameter) were counted, greater than 80% of dust devils in the medium category (3-16m) and all those in the large category ... were counted by the observer’. This, incidentally, is the only completeness estimation known to the present authors for terrestrial visual surveys. Hence the overall dust devil rate was probably a factor of a few higher than the 14 devils $\text{km}^{-2} \text{ day}^{-1}$ above, and seems consistent with the ~ 100 devils $\text{km}^{-2} \text{ day}^{-1}$ indicated by Pathare et al. (2010).

A diameter criterion is somewhat straightforward to implement with appropriate preparation – visual data gives the angular width of a target, thus its range must be known by stereo imaging, by geometry (e.g. exploiting a raised imaging platform to derive range from elevation) or by comparison with known landmarks.

The radiometric criterion of detecting dust loading is rarely defined, and is surely variable depending on illumination conditions and visibility (e.g. the background atmospheric dust loading). It also depends on observing wavelength or whether human observers use polarizing sunglasses, for example. It follows that, for a given dust loading of particles/ m^3 (assumed uniform within a dust devil; note that the extinction or area/volume depends also on the particle size), the opacity, or column optical depth, will depend on the size of the dust devil. Thus for a given optical contrast detection criterion, larger devils are easier to detect.

It would be desirable in stating observed dust devil counts to document an absolute contrast threshold used in the detection, that can at least crudely be related to dust loading. In practice, a relative contrast threshold may be used, which may depend on the image noise properties and/or the variation in the sky or ground background. In this connection it may be noted that dust devils are often – perhaps counterintuitively – easier to detect against a terrain background than against the sky.

It may be noted in passing that dust devil shadows are instrumental in Mars orbital studies of dust devils. Not only can the height of dust devils be measured this way, and in some cases the opacity can be measured via the shadow contrast, but many surveys rely on the shadows to detect dust devils as a pair of features (a bright circle, with a quasi-linear dark shadow). In other words, the presence of a shadow adjacent to a dust devil feature enhances the probability of detecting the feature (or equivalently lowers the size or opacity threshold for detection). This effect, plus the increased line-of-sight contrast for dust devil columns seen from above (Lorenz, 2014) may explain in part the slightly higher-than-trend counts of Mars dust devils seen from orbit (figure 3).

3.2 Vortex detection in Simulations

Large Eddy Simulations (LES - see chapter on LES modeling by Spiga) can reproduce vortex structures under conditions similar to those in which they are seen in nature. Simulations expose the full fields of (computed) pressure and velocity, so while vortices can be detected by inspection by a human operator, for efficient gathering of statistics, an automatic vortex detection criterion must be defined. Practically, as for field data, a pressure drop

makes a useful first-order criterion, but in addition a vorticity criterion is employed. Vorticity is defined as the curl of the flow velocity vector \mathbf{u} , i.e. $\vec{\omega} \equiv \nabla \times \vec{u}$. The vorticity in a surface element with area δA is related to the flow's circulation Γ (the line integral of the velocity around that element) simply as $\omega \delta A = \Gamma$. For the 'wall' of a dust devil, with diameter D and circumferential windspeed u , the circulation is $\Gamma = \pi u D$, and the vorticity $\omega = 4u/D$. Note that the vorticity defined at the wall this way not only has the same dimensions as the spin rate, but a value that differs only by a factor (the spin rate R is simply $u/\pi D$, thus $R \sim \omega/12$).

Ohno and Takemi (2010) report vortex formation and evolution in an LES with a 1x1km domain and a horizontal resolution of 3m, with a CBL height of 800m and a surface heat forcing of 0.24 Kms^{-1} (i.e. $\sim 290 \text{ Wm}^{-2}$, typical of desert conditions on Earth). They find after model convergence that 225 vortices were detected (with a 10 Pa pressure drop threshold, and a vorticity threshold ζ of 0.15 s^{-1}) in a 2000s period. If we extrapolate to a typical sunny day (i.e. ~ 4 hrs or 15,000s of such strong heating), then this corresponds to 1600 vortices per km^2 per day. Raasche and Franke (2011) show results for a 4x4km domain and 2m resolution (as well as a smaller run at 1m resolution) with a CBL of 700m and 0.24 Kms^{-1} surface heating. They used a vortex detection threshold of $\zeta > 1 \text{ s}^{-1}$ and $\Delta P > 4 \text{ Pa}$ and found 25,000 vortex tracks in a 5400s run. This corresponds, given their 16 km^2 model domain, to ~ 1500 tracks/ km^2 in the run, or ~ 4500 vortices per km^2 per day. These LES vortex results are plotted in figure 2 – because the core pressure drops may correspond to intensities below typical field dust-lifting thresholds, many of these vortices would not be visible in nature, and so the frequencies are somewhat higher than field measurements of dust devil occurrence. The simulations appear broadly consistent with the highest counts of visible dust devils (i.e. those showing the smallest dust devils).

3.3 Vortex Detections in in Meteorological time Series Data

Dust devil passage manifests itself in meteorological data by several clear signatures (e.g. Sinclair, 1973 ; Ryan and Lucich, 1983; Ringrose et al., 2003, 2007 ; Tratt et al. 2003) - most notably a pressure drop lasting a few seconds to hundreds of seconds and a rotation of the wind direction. Wyett (1954) noted a dust devil passage in a recording barograph at an airport meteorology station, and Lambeth (1966) documented about 20 pressure drops with an array of six stations in a 4-month period at White Sands, New Mexico. The low detection efficiency is likely due to a high threshold for triggering the chart recording (i.e. while the effort was devoted to acquiring in-situ data, the detection was optical).

For comparison with Mars in-situ detections, where meteorological data were recorded quasi- continuously and examined post-hoc for vortex signatures (Ryan and Lucich, 1983; Murphy and Nelli, 2002; Ellehoj et al., 2010), a comparable measurement approach is needed for Earth, with high-cadence meteorological data acquired at a fixed station for weeks or months.

After some initial experiments (yielding a 0.6mb devil in a 3-day survey reported in Lorenz, 2010) new measurements of this type have been made, enabled by the availability of small pressure loggers using flash memory to store the \sim Gbits of data required for multi-week multi-Hz sampling (Lorenz, 2012b; Lorenz, 2013a). A preliminary inspection of data from a trial field campaign at El Dorado Playa in Nevada (Lorenz, 2013a) suggested detectable encounter rates ($>0.3 \text{ mbar}$) on average of 1.3-2.6 per day. More systematic evaluations recording more than a hundred candidate events (Lorenz and Lanagan, 2014) and indeed some thousands of events (Lorenz and Jackson, 2015) have been conducted.

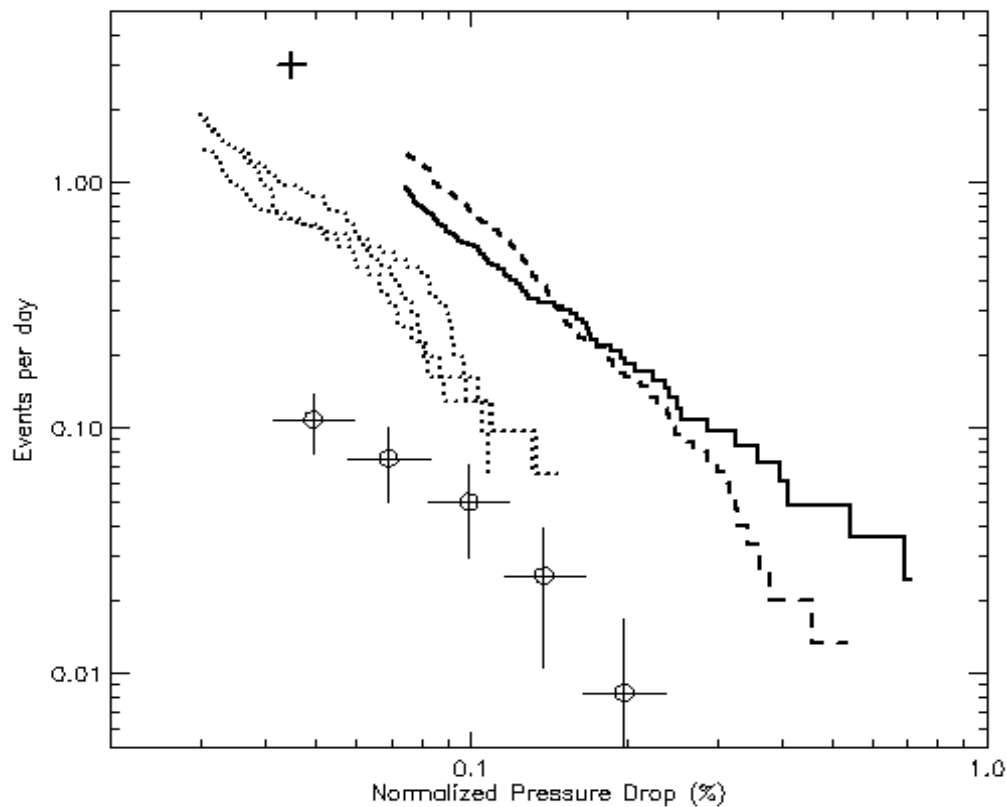


Figure 4. The intensity of vortex encounters at fixed stations on Mars (Pathfinder – solid line; Phoenix – dashed line and cross) and on Earth (El Dorado playa – Lorenz and Lanagan, 2014 – dotted line). The double-logarithmic axes show power-law populations as straight lines. The likely incomplete survey by Lambeth (1966) at White Sands is shown by the circles with $1\text{-}\sigma$ error bars. Populations are expressed as cumulative numbers of events per 100 days with amplitude greater than the abscissa. Since Mars ambient pressures are $\sim 100\text{x}$ smaller than Earth's, the population is shown as a normalized pressure. This metric is roughly proportional to vortex speed.

There has been some debate regarding the optimal way in which to parameterize or even how display the distributions of dust devil pressure parameters, with different groups advocating power-law or exponential fits, cumulative or differential histograms (Pathare et al. 2010, Lorenz 2011, Kurgansky 2012). Since different processes may give rise to different populations, answering these questions is not merely an academic subject.

With 252 million pressure readings, Jackson and Lorenz (2015) recovered more than 1,000 putative dust devil pressure drops during a two-year terrestrial field campaign and were able to compare different parametric fits to the histogram of pressure drops. Figure 5 shows data from that study which illustrates the pressure drop histogram, with bin sizes determined using Knuth's Rule, a binning scheme that uses a Bayesian framework to determining bin size. Neglecting small drops (with $\Delta P < 0.2$ hPa), that study found that a power-law fit to the histogram (with an index of -2.59 ± 0.11) gave a reduced chi-squared nearly half that for an exponential fit (with an e-folding pressure of 0.15 ± 0.01 hPa), which argues that the power-law is statistically a better fit.

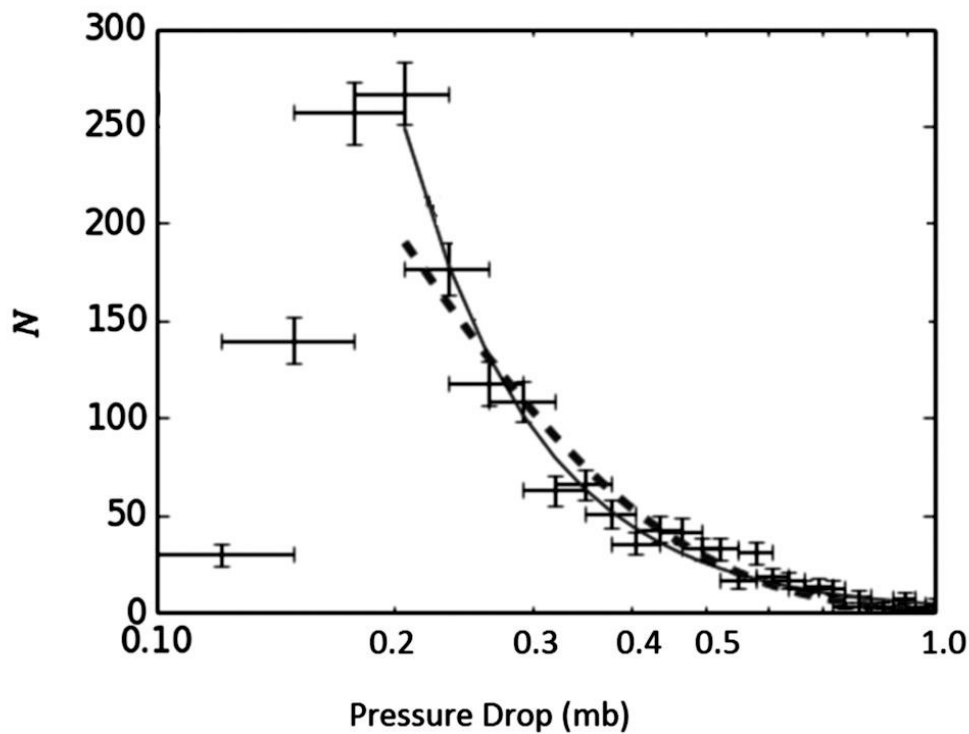


Figure 5. The aggregated counts of Jackson and Lorenz (2015) shown as a differential population function with bins sized to maximize information content. A power law fit is shown with the solid line, and an exponential with a dashed line. Both candidate functions deviate from observations below 0.2 mb, either due to an intrinsic minimum intensity of the population, or low detection efficiency for events near the noise level.

Jackson and Lorenz (2015) also leveraged their large number of recovered pressure drops to investigate how the number of detections influenced the resulting fits and determine how robustly a given power-law index could be recovered if fewer detections were made. Randomly selecting sub-samples of the full, recovered population and fitting a power-law to the each resulting histogram, the study found that smaller populations of drops could give wildly different power-law fits and, to retrieve the final best-fit to the full sample, at least 75% of the full sample would have had to be recovered. This result shows that small number statistics could easily explain why analyses of smaller samples give different functional fits to the dust devil distributions.

Finally on this topic, we may remark that the cumulative plot has the virtue that even very meagre datasets can be meaningfully portrayed and compared in this manner. Lorenz and Radebaugh (2016) report results of only 1-1.5 days of observation with a pocket pressure logger at a high-elevation site (~3600m) in the Argentine Puna. Meteorological and/or geological conditions at this site seem to yield particularly abundant and/or intense dust devils. Even though only three events were detected, the cumulative counts (figure 6) clearly suggest a higher level of activity, with 95% Poisson error bars barely overlapping with the benchmark Eldorado counts of Lorenz and Lanagan (2014).

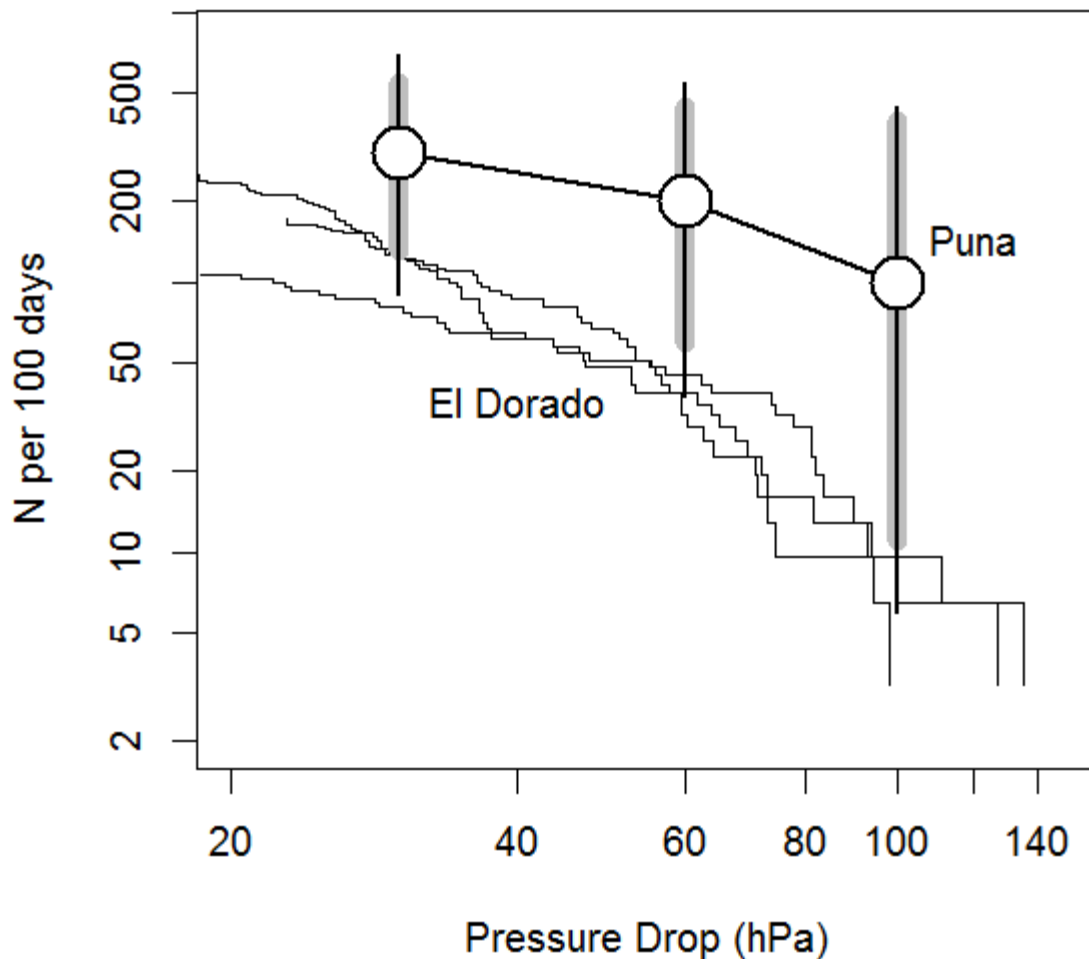


Figure 6. Counts (circles) of high-elevation dust devils from only 1-1.5 days of observation in Argentina (Lorenz and Radebaugh, 2016). The thick grey bars are 90% and the thin solid bars 95% confidence limits, suggesting a strong probability that the apparently high incidence of encounters was not random. A cumulative plot allows even only three events to be meaningfully portrayed.

3.4 Reconciling Vortex Detections and Observed Dust Devils

Lorenz (2014) showed with a Monte Carlo model that the occurrence frequency of in-situ vortex detections (via pressure drop) measured on El Dorado playa (Lorenz and Lanagan, 2014; Jackson and Lorenz, 2015) could be related to the observed number of dust devils seen in visual surveys (e.g. Pathare et al., 2010). The model introduced random vortices into an ‘arena’ containing a virtual pressure sensor. The vortices were drawn from a specified (truncated power law) diameter and core pressure drop distribution, with an assumed velocity distribution and a longevity related to diameter, and the detection process (pressure drop threshold exceedance) was simulated to recover the observed (‘sample’) population as a function of the underlying complete population. Unsurprisingly, the visual detections had to be less abundant than the full vortex population, indicating that only a fraction of vortices form visible dust devils. In the case simulated, the vortex population was considered with core pressure drops as small as 0.1 hPa, but only those of 0.3 hPa or higher were assumed to be dusty. (The simulation assumed that all vortices with intensity above this threshold would have been detected optically – this makes some assumptions about

the acuity and efficiency of the observing process.) The dust devil generation rate consistent with the observed detections ($\sim 2/\text{day}$ at 0.2 hPa) is shown in figure 2, and also appears consistent with an ‘asymptotic’ underlying vortex population of a few hundred per km^2 per day.

Some insight into the relative numbers of dusty and dustless devils is afforded by field measurements at El Dorado. Lorenz and Jackson (2015) and Lorenz et al. (2015) report using pressure loggers with solar cells to detect dust devils – the vortex signature is indicated as a pressure drop, which is accompanied in about 40% of cases by a drop in measured sunlight due to shadowing by lofted dust. As shown in Lorenz and Jackson (2015)’s field data, and modeled by Mason et al. (2013), sometimes a double-shadow is seen in near-diametric encounters with devils with well-defined cylindrical ‘walls’ of dust. Lorenz and Jackson (2015) also note an occasional increase in solar flux, due to dark sky in the anti-sun direction being occupied by a scattering dust plume. Lorenz and Jackson (2015) found that about 40% of detected vortices (using a 10-s average pressure drop of 0.2 hPa as a detection threshold) had no measurable ($\sim 0.2\%$) accompanying drop in sunlight, and 60% had a drop less than 1% (which approximately corresponds to a human visual detection threshold). This does not mean, however, that 40% of vortices have no dust. For example, no shadow was measured for near-misses with the devil to the antisunward direction of the sensor.

We will for the moment introduce the concept of a pressure-detection cross section (see later). Vortex models (see chapter by Kurgansky et al.) indicate pressure falls off from the core as $\sim 1/([2x/D]^2+1)$. If the pressure drop detection threshold is ~ 0.2 hPa, and the core pressure drop is $\sim 0.7\text{--}2.7$ hPa, then the dust devil can be detected in the pressure time series at a miss distance of $x < 0.7D$ to $1.7D$ in any direction. In contrast, while in typical conditions a shadow might be detected at a sunward distance of as far as $\sim 6D$ (e.g. for a height/diameter of ~ 5 and a sun elevation a little less than 45°). Thus all sunward pressure-detected vortices would have detectable shadows, but not all shadow-detected devils would have a measureable pressure signature. On the other hand, the shadow is detected only for miss distances less than $0.5D$ in the antisunward direction. Thus for uniformly-distributed miss distances, the entire sunward half of the pressure-dip events are measured to have shadows if dust is present, whereas only a fraction ($0.5/0.7$ to $0.5/1.7 = 30\text{--}70\%$) of the antisunward half do, or $65\text{--}85\%$ of the total. Thus for the observed 60% of shadows when vortices were detected, this geometric correction suggests that in fact $70\text{--}95\%$ of detected vortices should have had observable amounts of dust.

3.5 Dust Devil Trails as a Population Metric

Although dust devil tracks or trails have been observed on Earth (see review chapter by Reiss et al., they are comparatively rare, and so we consider here only trails at Mars where their quantitative treatment may be useful.

It is commonly observed on Mars that dust falls out of the atmosphere onto surfaces, altering their color or brightness with a typical characteristic timescale of the order of 100 sols (although there are of course regional, seasonal and interannual variations). Arvidson et al. (1983) noted that dark material exhumed by the Viking lander sampling arm brightened on this timescale. Kinch et al. (2007) suggested a monolayer of dust accumulated on rover camera calibration targets in about 100 sols. The Pathfinder rover solar panels lost capacity at a rate of about 0.3% per sol (Landis and Jenkins, 2000) or an e-folding timescale of about 200 sols, but considering that the dust is partly reflective in the solar array bandpass, this timescale is probably larger than that to accumulate unity optical depth.

Thus to a first order, the observation of a dust devil track on the surface of Mars indicates a vortex passage intense enough to remove dust in the last 100 sols. Dust devil tracks can in fact be recognized (after the fact, Lorenz and Zimelman, 2014) in the first Mariner 9 images from 1972 that show sand dunes on Mars. However, their detailed quantification awaited higher-resolution images that became available after 1998.

In Hellas, the number of observed dust devil tracks in a survey by Balme et al. (2003) increased from ~ 0.6 to 3.5 km^{-2} over about 30 sols (between the intervals of $L_s = 285\text{--}300$ and $L_s = 300\text{--}315$). This corresponds to a track generation rate of about 0.1 km^{-2} per day. More typically the generation rate was about a fifth of this rate. Verba et al. (2012) find similarly at Gusev in 2006–2008 a peak formation rate of $0.103 \text{ tracks km}^{-2}/\text{sol}$, although as low as 0.0011. At Russell crater, track formation was rather more frequent, $0.04\text{--}0.95 \text{ tracks km}^{-2}/\text{sol}$.

Verba et al. (2012) report dimensions of dust devil tracks in Gusev crater, finding average widths of 40 m and lengths of 2.5 km. The area swept by an ‘average’ track is therefore 0.1 km^2 . The formation of a 0.1 km^2 trail at a rate of 0.1 per km^2 per day implies a typical interval between cleaning events seen by a given point of 100 days during the most intense part of dust devil season, and 500 days more typically.

This 100–500 day interval is reassuringly close to that of dust clearing events indicated at Spirit. This agreement between track formation rate, dust clearing, and observed vortex distributions again supports the notion that dust devils are responsible for clearing events.

While the notion of ‘average’ for a highly skewed population requires considerable care, it is instructive to compare this average trail area of 0.1 km^2 with the area swept by a typical dust devil. Lorenz (2013) determines a longevity of a dust devil diameter d (in m) as $\sim 40d^{0.66} \text{ s}$, or for a 40 m dust devil, about 8 min. With a $5\text{--}15 \text{ m s}^{-1}$ ground speed typical of dust devils (e.g. Reiss et al., 2014a), a devil would migrate 2–6 km, spanning the average length noted by Verba et al. (2012). This suggests some overall consistency, and circumstantially implies that dust devils may be able to form trails for most of their observed lifetime. In this connection, Raasch and Franke (2011, their figure 6) plot the time histories of two vortices in a Large Eddy Simulation (LES) model of terrestrial dust devils: the two vortices were tracked over 500 and 600 s respectively, and had core pressure drops exceeding 20 Pa (a likely dust-lifting threshold) for over 80% of their lifetime.

Verba et al. (2012) note that the population of observed tracks are wider than observed devils. As figure 7 shows, HiRISE observations of track widths peak at around 40–60 m across, with a mean of 56 m ($N = 640$), whereas the dust devils observed by the Spirit rover ($N = 480$) are generally between 10 and 20 m in diameter (see e.g. Greeley et al., 2010). While there may be some systematic differences in detection efficiencies, this difference is suggestive that track formation is favored for large devils. While it is possible that larger devils are more intense (i.e. ΔP and tangential windspeed correlate with diameter, such that larger vortices are better able to lift dust), modeling of terrestrial dust devils finds no evidence of correlation (Lorenz, 2014).

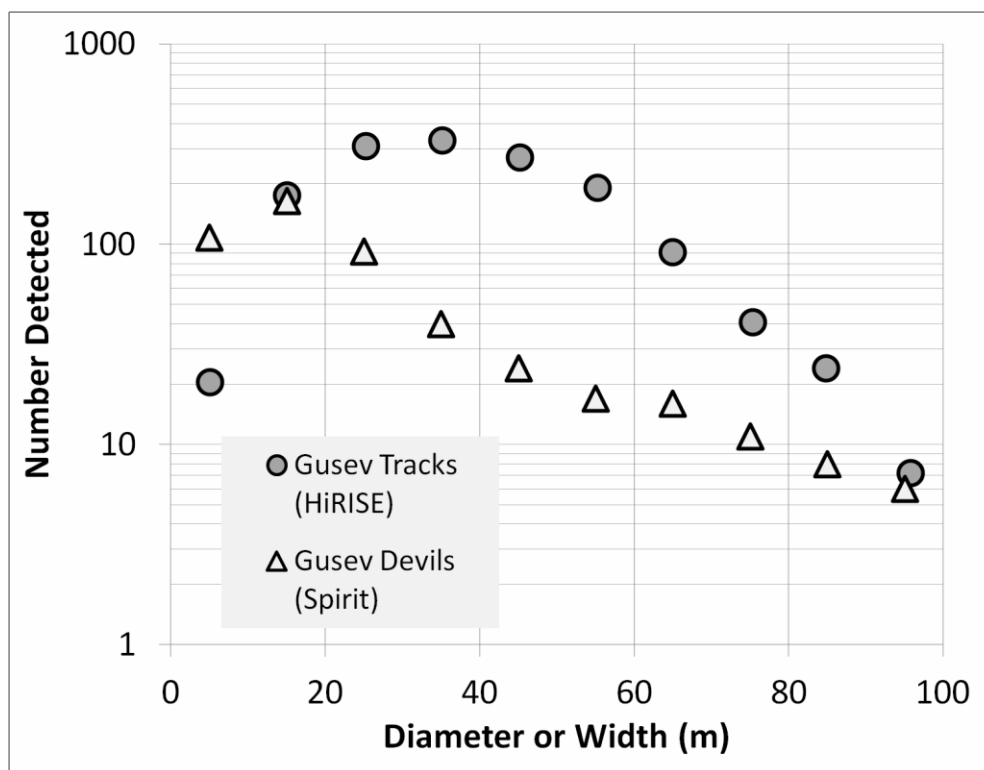


Figure 7. Gusev dust devil diameters compared with Gusev dust devil track widths. Since the HiRISE imaging resolution is of the order of 1m or better, image resolution should not be the main reason for the different distributions: it seems larger dust devils may be more effective at forming trails at this site, or that the path over which dust is removed is three times larger than the visible dust column.

4. Statistics on Earth and Mars

Here we address the question of whether Martian dust devils are larger than those on Earth. As noted earlier, the skewed size distribution makes this a subtle question. A formal assessment can in principle be made non-parametrically (i.e. without fitting a model function), by the application (for example) of a Kolmogorov-Smirnov test, which measures the probability that two different populations are drawn from distinct underlying distributions. However, the combination of coarse binning, and the lack of truly equivalent datasets (i.e. observations with the same survey areas, contrast criteria etc.) means only a somewhat informal answer (yes) can be given in practice.

The reason for caution will be apparent in figure 8, which shows convincingly that the Ryan and Carroll (1970) dust devil population indicates much smaller dust devils than the Gusev survey by Greeley et al. (2006) – the peak in the function (the modal diameter) is about 20 times larger in the Gusev survey. But the terrestrial measurements were made over a short period in a very small survey area, so preferentially detect small devils. This survey area/size/number dependence is the foundation for the variations in detected numbers shown in figure 2, and is evident when an orbital survey at Mars is considered, also in figure 10. It might be concluded that dust devils seen from orbit at Mars are much larger than those seen from the Spirit rover – and while that is true, it is merely a result of the poor efficiency of detection of small devils from long ranges. In other words, Mars dust devils typically look larger, because we typically are looking from further away.

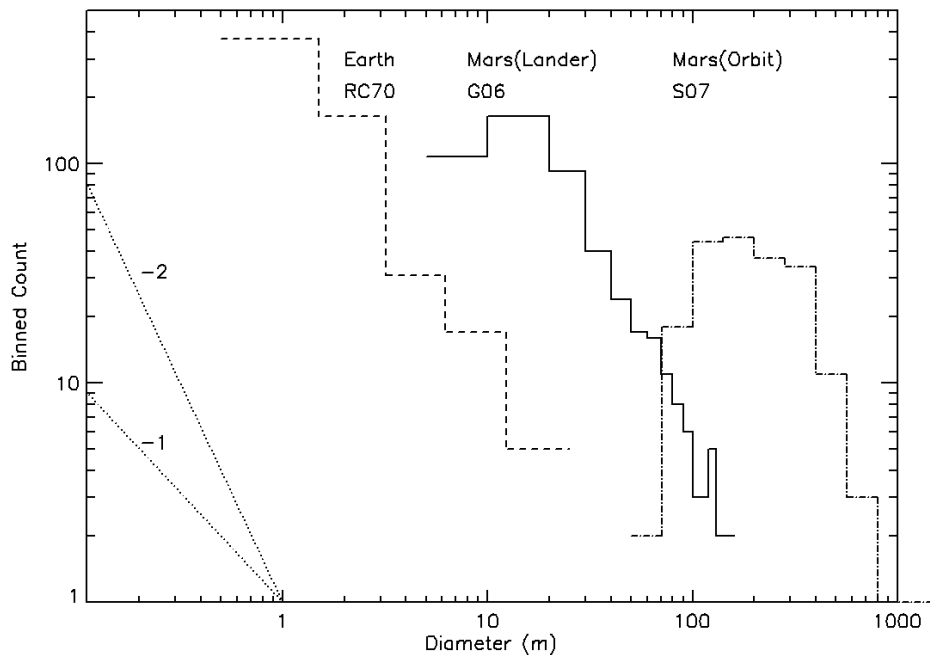


Figure 8. Plotted are the binned counts of dust devils on Earth (Ryan and Carroll, 1970), and on Mars from the Spirit rover (Greeley et al, 2006) and from Mars Express (Stanzel et al., 2007). Differential power law slopes of -1 and -2 are shown at right. From this plot one might conclude that Martian dust devils are larger (the modal diameter on Mars is ~15m, while more like ~1m on Earth), although it is also clear that one might also conclude that dust devils seen from orbit are much larger than those seen from the ground, by a similar factor. Thus it should similarly be noted that the Ryan and Carroll study was over a very small (<1km²) area, and so observed many small dust devils.

This distance bias could be addressed with a model of the observing process to correct for detection thresholds, but to a first order can be examined by comparing (figure 9) two datasets with somewhat similar conditions, namely the Tucson survey by Sinclair (1969) – over a ~500 km² area, and that at Gusev, over a similar area. Unfortunately the coarse binning of the terrestrial data makes the comparison challenging (the curves could be moved up or down if the observing period were different), but the modal diameter appears to be ~3 times larger on Mars. An unbinned (or at least finely-binned) terrestrial dataset may permit a more confident answer of this question.

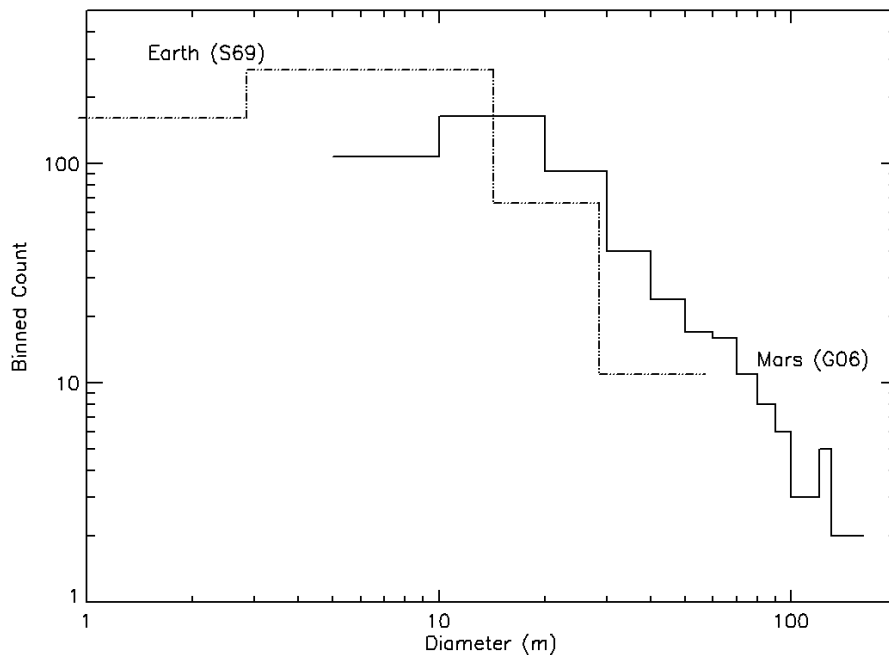


Figure 9. A ‘Devil’s Advocate’ plot, to – not altogether seriously – propose the possibility that Mars and Earth devils are actually the same size. These data, from Sinclair’s (1969) study at Tucson, and the Spirit observations of Greeley et al. (2006) involve roughly comparable survey areas, and so the bias in the terrestrial survey to smaller devils is not as severe as in the Ryan and Carroll example: in this instance the modal diameter on Earth is more like 5m, only a factor 3 smaller than on Mars. It is notable that the largest devil seen in the Mars set is larger than that at Earth, but perhaps a longer survey on Earth (pushing the curve upwards) would allow the expected number of detections of larger devils on Earth to rise above 1.

While the diameter distributions shown in figure 9 are merely suggestive of a larger modal diameter, it is certainly the case that the largest devil diameters reported are larger on Mars – see table 1. Those summary statistics also suggest that Martian dust devils have a higher intensity (in the sense of relative pressure drop, expressed as a percentage of ambient) – again, the highest values recorded by surveys are at Mars, although possibly some targeted encounters on Earth that penetrate the very core of the devil may be higher yet. Note that the normalized pressure drop corresponds to a vortex wind speed – the atmospheric density contribution to dynamic pressure is proportional to ambient pressure. Encounters with a given threshold of normalized pressure drop (0.1%, 0.5%) appear to occur more frequently on Mars than at typical terrestrial locations, although the high-elevation site studied by Lorenz and Radebaugh (2016) may be an exception. The maximum number of dust devils per km² per day on Mars, from the Spirit rover during its first season (Greeley et al., 2010) appears lower than the Ryan and Carroll (1970) value, although this may be an observational limit since the area surveyed was rather larger, exposing fewer small devils, than that terrestrial survey (see section 3.1).

Table 1. Properties of Dust Devil Populations

Characteristic	Unit	Earth	Mars	Notes
Largest Diameter Observed	(m)	>100	1,650	1,2
Tallest Height Observed	(m)	~2,500	20,000	1,3
Maximum Field Frequency	(km ⁻² day ⁻¹)	300	51	4,5
Largest Pressure Drop Observed	(Pa)	450*	4.8	6,7
(Normalized to Background)	(%)	0.5	0.7	6,7
Interval for 0.5% Encounters	(days)	>300	20-100	8,9
Interval for 0.1% Encounters	(days)	~10	1	8,9

1 Snow & McLelland (1990) 2. Stanzel et al. (2007) 3. Fenton and Lorenz (2016) 4. Carrol and Ryan (1970) 5. Greeley et al., (2010) 6. Sinclair (1973) 7. Murphy and Nelli (2002). 8. Lorenz and Lanagan (2014) 9. Lorenz and Reiss (2015)*this is the largest reliable value in a refereed journal. See Balme and Greeley (2006) note some unpublished theses by RIngrose and by Metzger which report 1000 and 1500 Pa respectively for Earth

5. Heuristic Metrics

Although our philosophy is that wherever possible, the effects of a dust devil population or the magnitude of a meteorological perturbation should be evaluated explicitly, it is worth discussing a couple of heuristic quantities used in the literature as approximations.

5.1 Pressure Cross Section

Some attempts to compare visual dust devil counts with in-situ meteorological detections (e.g. Moores et al., 2014) have invoked a 'pressure radius' distinct from an 'optical radius'. While in principle one can assess detection cross-sections in this way, we discourage this approach as it is only meaningful when integrated across a whole population. The problem is that the detection distance of a vortex (the 'pressure radius') depends not only on the actual vortex radius (i.e. that of the 'wall', the optical radius, where the windspeed is a maximum and the pressure drop is half that at the center) but also on the pressure detection threshold, and on the core pressure drop. The core pressure drop and the diameter are not necessarily correlated, and thus the average over the full population of these properties is difficult to estimate accurately.

As discussed in section 3.4, for terrestrial surveys a pressure radius of ~1.5-3.5 optical radii is a reasonable range which might be considered for the most crude calculations. However, the correlation of diameter with longevity needs to be considered in any attempt at an accurate reconciliation of visual and in-situ records (e.g. Lorenz, 2014).

5.2 Area Fraction of Dust Devils

A common metric in the literature is the 'area fraction' – the instantaneous or averaged area covered by dust devils (presumably defined by their optical diameter). This is a more useful metric in some senses than a simple count of dust devils, in that larger dust devils are given larger 'weighting'. Thus a total dust flux derived from multiplying an 'average' flux per unit area in dust devils and the area fraction should be more representative than some 'average' dust flux per devil multiplied by the number of devils. In an ideal world, of course, these averages would be accurately computed and the results would be equivalent, but this is rarely the case and indeed it is all but impossible to know how well such quantities are evaluated.

If we adopt a value of 100/km²/day with a minimum diameter of 1m, and assume that a dust devil has a longevity $t = 40d^{0.66}$ s, then the fractional area covered by dust devils can be calculated by integrating the time-area product $tpd^{2/4}$ over the population. If all dust devils were only 1m in diameter (i.e. a power law with an exponent of 0), then there are 100 dust devils per day per km² (10⁶ m²), each lasting 40 seconds, and each with an area of 0.75 m². Then the fractional area covered is $100*40*0.75/(86400*10^6) = 3x10^{-8}$.

If, instead, devil diameters follow a power law with exponents -1, -1.6 and -2, the resultant area fractions are 3×10^{-4} , 2.3×10^{-5} and 4×10^{-6} . It can be seen that these values are much higher than if all dust devils were small. As noted by Lorenz (2011), population-integral quantities such as total dust lifting or area fraction are dominated by the largest dust devils. Thus the notion of an 'average' dust devil requires exceptional caution, and perhaps should be avoided altogether, since such an average cannot be accurately determined from a small sample of the population.

For the -1.6 cumulative power law (favored by the Mojave data), the 2.3×10^{-5} fraction is reduced to 1.1×10^{-5} if the power law is truncated at 100m diameter (i.e. if one assumes there are no dust devils larger than this). Evidently, the fraction also scales directly with the density of devils ($100 \text{ km}^2/\text{day}$).

It is striking that the area fraction computed by integrating the observed parameters (-1.6 cumulative power law, $100 \text{ km}^2/\text{day}$) of 1.2×10^{-5} is very similar to the area fraction computed by Koch and Renno (2006). It follows, perhaps, that the -1.6 power law, truncated at ~1m at the small end, and some diameter of the order of 100-300m at the high end, is a reasonably good representation of the terrestrial population.

Greeley et al. (2010) report dust devils observed on Mars by the Spirit rover at Gusev crater over years: the densities observed were 51, 11 and 20 per km^2/sol with median diameters of 19, 24 and 39m respectively, average lifetimes of 129-170s and average speeds of 1.5-2.5 m/s. The Gusev data for 2006 was fit with a -2 differential power law (-1 cumulative), although the following two years appear to have steeper fall-offs.

The smallest size bin was 0-10m. If we adopt 5m as the minimum size, and a -1.6 cumulative power law as for Earth, but truncated at 500m, then we find for $N(>5\text{m})=20 \text{ dd}/\text{km}^2/\text{sol}$ that the area fraction occupied by dust devils is some 1.6×10^{-4} , essentially an order of magnitude higher than for Earth. The distinction appears largely due to the larger size of dust devils on Mars. This in turn is likely related to the thicker planetary boundary layer.

6. Statistical Properties of Dust Devil Counts

In so far as dust devils are relatively rare events, it is tempting to consider (and may be convenient to model) their occurrence as a Poisson process. For example, the P28 Eldorado dataset shown in figure 4 previously suggests a 1 mbar dust devil encounter may occur once every ten days or so, and thus has an occurrence frequency of $\sim 0.1/\text{day}$. This is of course not the same as a rate of 0.04 /hr, since dust devils typically do not occur during most of a 24 day period. Thus we implicitly consider a periodic or conditional factor in dust devil frequency – most usually by considering an 'active' period of only 6-8 hours per day. Thus during the active part of the day, 10-11am local solar time to 5-7pm or so, the recurrence rate is about 0.015 /hr. This is quite a small value, and thus one would not expect two devils to occur in the same hour if they were truly independent events. Similarly, one would expect images of large areas showing multiple dust devils to be progressively less and less common as the number of dust devils increases.

This, however, is not what is observed. A survey of Mars Reconnaissance Orbiter Context Imager (CTX) images of Amazonis Planitia on Mars (Fenton and Lorenz, 2015) shows not the monotonically-declining frequency of higher-populated images, but rather a bimodal distribution, with either a handful of dust devils, or about 30. The images cover areas of 4000-8000 km^2 at a resolution of 6m/pixel, with dust devils being recognized for minimum diameters of 30-60m.

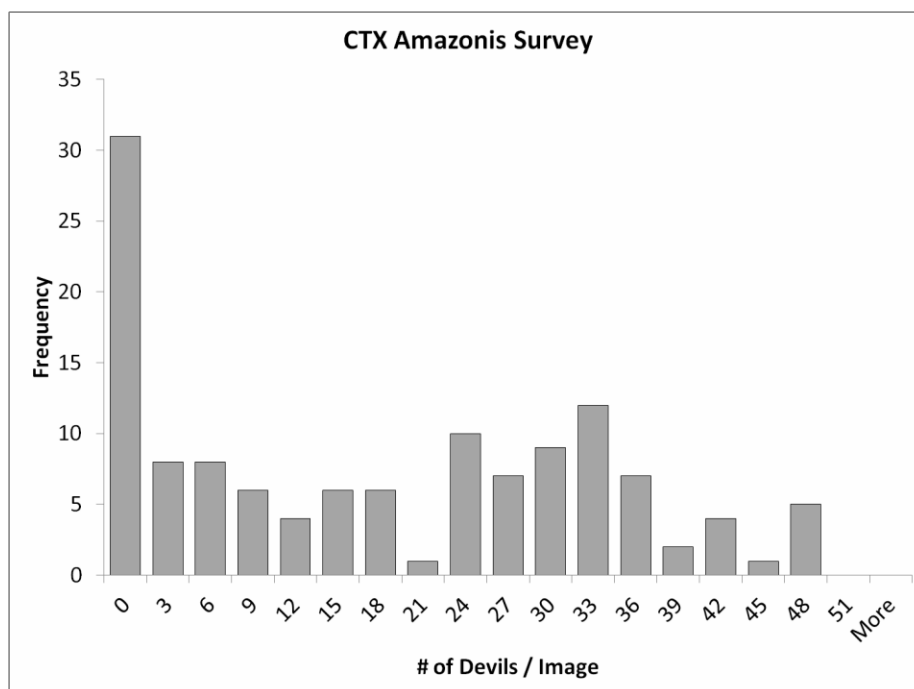


Figure 10. The number of dust devils seen in the very active Amazonis Planitia area of Mars with the CTX camera (Fenton and Lorenz, 2015). CTX images span an area of 4000-8000 km² and the corresponding devil diameters are some tens of meters. The clear bulge in the histogram for 24-36 devils/image is striking, and shows that dust devil appearances over ~100km ranges are correlated, in that favorable conditions must simultaneously apply over such a large region.

Since dust devil vortices occur in a set of favorable meteorological conditions (convective heating, with moderate wind shear), simultaneous dust devils are in fact quite common. Furthermore, occurrence of dust devils (or dustless vortices) at regular intervals – typically 5-20 minutes – associated with the advection of a quasi-regular cellular pattern of boundary layer convection over a meteorological station have been noted (e.g. Lorenz and Christie, 2015). Trains of regularly-spaced dust devils are sometimes reported (see Fenton and Lorenz, 2015 and references therein).

The correlated occurrence of dust devils makes population measurements challenging, in that a short observing interval may encounter a 'lucky' day with many events, or a quiet day when conditions are for some reason unfavorable.

7. Summary and Conclusions

From this review of population studies, we can conclude the following:

When evaluating the broad influence of dust devils on the martian or terrestrial atmosphere, population-weighted statistics should be considered to the extent possible. The apparently skewed nature of the dust devil population and the steep dependence of their dust-lifting capacity on their physical properties mean that 'typical' or 'average' values may not be adequate. For instance, lab experiments reported in Neakrase et al. (2006) suggested that the dust flux from a vortex scales exponentially with a vortex's pressure drop, meaning the deepest (largest) but rarest devils dominate the martian dust flux, and the flux estimated by considering the "average" devil could be incorrect by orders of magnitude.

The *observed* populations of Martian dust devils indicate a larger diameter than for Earth. This is reflected not only in the largest diameters (and heights) reported in various datasets, but also in sample statistics such as the median. It is not, however, firmly established whether either Mars or Earth samples are 'complete' in the sense of efficiently detecting the smallest devils. Thus these statistics should be used with some caution, although somewhat-comparable surveys suggest Martian dust devils may have a modal diameter a factor of ~ 3 larger than Earth's.

If dust devil height and diameter are correlated (as they appear to be), and if the ultimate limit on dust devil height is the thickness of the planetary boundary layer, then it follows from measurements of the latter (usually several km, in some cases more than 10km, compared with a maximum of 2-4km on Earth) that the upper limit on dust devil diameter will be larger on Mars than Earth by a factor of ~ 4 .

Available data do not yet indicate fundamental differences between Earth and Mars on the correlation between diameter and longevity. This correlation is important in that it influences the extent to which dust-lifting may be dominated by the largest, rarest dust devils.

Some recommendations in future analysis or re-analysis of observational datasets (field or remote sensing) are as follows:

The 'stopping rule' in surveys should be reported. As an example, did field observations extend for a predetermined period (e.g. 'stop at 6pm, no matter what') or did they terminate when there appeared to be nothing happening (e.g. an hour since the last dust devil was seen)? Similarly the criteria for selecting remote images for study should be given (and the number of images examined in which dust devils were not detected should be reported). Detection criteria should be quantified as well as possible (e.g. contrast threshold) and methodology in visual surveys reported (e.g. counts made in a 1-minute horizon sweep at 15 minute intervals, or continuous surveillance, etc.).

Survey completeness should also be assessed to the extent possible. For surveys using barometric time series, injection and recovery of synthetic dust devil signals can reveal the efficiency of a chosen detection scheme and its dependence on the signal's properties. Similar injection efforts may be possible for surveys involving orbital or in-situ visual data. For both types of surveys, images of identified dust devils could be mixed together with control images without identified devils and contrast ratios adjusted. The workers surveying the visual data for devils could then attempt to sift the real devils from the control images, allowing the detection efficiency to be evaluated.

Binning into size categories may be the only practical approach in some cases, but in general binning is to be avoided as information is lost. Tabulation of raw times, longevities, diameters, speeds etc. for individual devils is most useful. In particular, data should be archived and made available to other workers, a requirement in other fields.² In graphical presentation, a cumulative plot on logarithmic axes can be useful.

² The Planetary Atmospheres Node of NASA's Planetary Data System provides support for researchers who wish to archive their dust devil data – <http://atmos.nmsu.edu/atmos-home.html>.

References

- Arvidson, R.E., Guinness, E.A., Moore, H.J., Tillman, J. and Wall, S.D., 1983. Three Mars years: viking lander 1 imaging observations. *Science*, 222, pp.463-468.
- Balme, M.R., Whelley, P.L., Greeley, R., 2003. Mars: Dust devil track survey in Argyre Planitia and Hellas Basin. *J. Geophys. Res.* 108, 5086. <http://dx.doi.org/10.1029/2003JE002096>.
- Broersen, T., 2013. Quantification of soil erosion by dust devil in the Jordan Badia. MSc Thesis, University of Utrecht, The Netherlands
- Carroll, J.J. and Ryan, J.A., 1970. Atmospheric vorticity and dust devil rotation. *Journal of Geophysical Research*, 75(27), pp.5179-5184.
- Fenton, L. and Lorenz, R., Dust devil height and spacing with relation to the Martian planetary boundary layer thickness, *Icarus*, 260, 246–262, 2015
- Greeley, R., Whelley, P.L., Arvidson, R.E., Cabrol, N.A., Foley, D.J., Franklin, B.J., Geissler, P.G., Golombek, M.P., Kuzmin, R.O., Landis, G.A. and Lemmon, M.T., 2006. Active dust devils in Gusev crater, Mars: observations from the Mars Exploration Rover Spirit. *Journal of Geophysical Research: Planets*, 111(E12). doi/10.1029/2006JE002743
- Jackson, B. K. and R. D. Lorenz, 2015. A Multi-Year Dust Devil Vortex Survey Using an Automated Search of Pressure Time-Series, *Journal of Geophysical Research, J. Geophys. Res. Planets*, 120, doi: 10.1002/2014JE004712.
- Kinch, K.M., Sohl-Dickstein, J., Bell III, J.F., Johnson, J.R., Goetz, W., Landis, G.A., 2007. Dust deposition on the Mars Exploration Rover Panoramic Camera (Pancam) calibration targets. *J. Geophys. Res.* 112, E06S03. <http://dx.doi.org/10.1029/2006JE002807>.
- Kurgansky, M. V., 2006. Steady-State properties and statistical distribution of atmospheric dust devils, *Geophysical Research Letters*, 33, L19S06
- Kurgansky, M. V., A. Montecinos, V. Villagran and S. M. Metzger 2010. Micrometeorological Conditions for Dust-Devil Occurrence in the Atacama Desert, *Boundary Layer Meteorology*, 138, 285–298.
- Kurgansky, M. V. 2012. Statistical distribution of atmospheric dust devils, *Icarus*, 219, 556-560
- Landis, G.A., Jenkins, P.J., 2000. Measurement of the settling rate of atmospheric dust on Mars by the MAE instrument on Mars Pathfinder. *J. Geophys. Res.* 105, 1855–1857.
- Lorenz, R. D., 2009. Power Law of Dust Devils on Earth and Mars, *Icarus*, 203, 683-684
- Lorenz, R. D., 2011. On the Statistical Distribution of Dust Devil Diameters, *Icarus*, 215, 381-390
- Lorenz, R. D., Pressure Drops in Dust Devils : Earth and Mars, *Planetary and Space Science*, 60, 370-375, 2012
- Lorenz, R. D., The Longevity and Aspect Ratio of Dust Devils : Effects on Detection Efficiencies and Comparison of Landed and Orbital Imaging at Mars, *Icarus*, 226, 964-970, 2013
- Lorenz, R. D. 2014. Vortex Encounter Rates with Fixed Barometer Stations : Comparison with Visual Dust Devil Counts and Large Eddy Simulations, *Journal of the Atmospheric Sciences*, 71, 4461-4472
- Lorenz, R. D. and P. D. Lanagan, 2014. A Barometric Survey of Dust Devil Vortices on a Desert Playa, *Boundary Layer Meteorology*, 53, 555–568. DOI 10.1007/s10546-014-9954-y
- Lorenz, R. D. and J. Zimbelman, 2014. *Dune Worlds : How Wind-Blown Sand Shapes Planetary Landscapes*, Springer, 308pp.
- Lorenz, R. D. and D. Christie, 2015. Dust Devil Signatures in Infrasound Records of the International Monitoring System, *Geophysical Research Letters*, 42, 2009–2014, doi: 10.1002/2015GL063237.
- Lorenz, R. and J. Radebaugh. 2016. Dust Devils in Thin Air : Vortex Observations at a High Elevation Mars Analog Site in the Argentinian Puna, *Geophysical Research Letters*, doi:10.1002/2015GL067412
- Mattsson, J.O., Nihlén, T. and Yue, W., 1993. Observations of dust devils in a semi-arid district of southern Tunisia. *Weather*, 48(11), 359-363.
- Melosh, H. J. 1990 *Impact Cratering : A Geologic Process*, Oxford University Press.
- Metzger, S., M. Balme and A. Pathare, 2009. Meteorologic Conditions and the Formation of Terrestrial Dust Devils, #1229, 40th Lunar and Planetary Science Conference, Houston, TX, March 2009.
- Moores, J.E., Lemmon, M.T., Kahanpää, H., Rafkin, S.C., Francis, R., Pla-Garcia, J., Bean, K., Haberle, R., Newman, C., Mischna, M. and Vasavada, A.R., 2015. Observational evidence of a suppressed planetary boundary layer in northern Gale Crater, Mars as seen by the Navcam instrument onboard the Mars Science Laboratory rover. *Icarus*, 249, pp.129-142.
- Murphy, J.R. and Nelli, S., 2002. Mars Pathfinder convective vortices: Frequency of occurrence. *Geophysical Research Letters*, 29(23). doi/10.1029/2002GL015214

- Neakrase, L. D. V., R. Greeley, J. D. Iversen, M. R. Balme and E. E. Eddlemon, 2006. Dust flux within dust devils: Preliminary laboratory simulations, *Geophysical Research Letters*, 33, L19S09. doi: 10.1029/2006GL026810
- Ohno, H., and T. Takemi, 2010: Mechanisms for intensification and maintenance of numerically simulated dust devils. *Atmos. Sci. Lett.*, 11, 27–32, doi:10.1002/asl.249.
- Oke, A. M. C., N. J. Tapper and D. Dunkerley, 2007. Willy-willies in the Australian landscape: The role of key meteorological variables and surface conditions in defining frequency and spatial characteristics, *Journal of Arid Environments*, 71, 201-215
- Pathare, A. V., M. R. Balme, S. M. Metzger, A. Spiga, M. C. Towner, N. O. Renno and F. Saca, 2010. Assessing the power law hypothesis for the size-frequency distribution of terrestrial and Martian dust devils, *Icarus*, 209, 851-852
- Raasch, S. and Franke, T., 2011. Structure and formation of dust devil-like vortices in the atmospheric boundary layer: A high-resolution numerical study. *Journal of Geophysical Research: Atmospheres*, 116(D16). doi/10.1029/2011JD016010
- Reiss D. 2016. First Observations of Terrestrial Dust Devils in Orbital Image Data: Comparison with Dust Devils in Amazonis Planitia, Mars. Abstract #2912, Lunar and Planetary Science Conference, Houston, TX 21-25 March, 2016.
- Ryan, J. A., and J. J. Carroll, 1970. Dust devil wind velocities: Mature state, *J. Geophys. Res.*, 75, 531–541
- Scargle, J., J. Norris, B. Jackson and J. Chiang, 2013. Studies in Astronomical Time Series Analysis. VI. Bayesian Block Representations, *The Astrophysical Journal*, Volume 764(2), article id. 167, 26 pp. doi: 10.1088/0004-637X/764/2/167
- Sinclair, P.C., 1969. General characteristics of dust devils. *Journal of Applied Meteorology*, 8(1), pp.32- 45.
- Sinclair, P.C., 1973. The lower structure of dust devils. *Journal of the Atmospheric Sciences*, 30(8), pp.1599-1619.
- Snow, J. T. and T. McClelland, 1990. Dust devils at White Sands Missile Range, New Mexico 1. Temporal and Spatial Distributions, *J. Geophysical Research*, 95, 13,707-13,721
- Stanzel, C., Pätzold, M., Williams, D.A., Whelley, P.L., Greeley, R., Neukum, G. and HRSC Co-Investigator Team, 2008. Dust devil speeds, directions of motion and general characteristics observed by the Mars Express High Resolution Stereo Camera. *Icarus*, 197(1), pp.39-51.
- Verba, C.A., Geissler, P., Titus, T., Waller, D., 2012. Observations from the High Resolution Imaging Science Experiment (HiRISE): Martian dust devils in Gusev and Russell craters. *J. Geophys. Res.* 115, E09002. <http://dx.doi.org/10.1029/2009JE003498>.